Supporting Information

Giant electric-field-induced strain associated with defect dipole in Fe-doped Barium Titanate single crystal activated by AC electric field

Chang Min Baek[a,1], Xiaoming Shi[b,1], Rokhyeon Kim[a], Ho-Yong Lee[c], Yunseok Kim[d], Jung Min Park[a], Houbing Huang[e,*], Dae-Yong Jeong[f,*], and Jungho Ryu[a,*]

[a] School of Materials Science and Engineering, Yeungnam University, Gyeongsan-si 38541, Republic of Korea

[b] Department of Physics and Advanced Research Institute of Multidisciplinary Science, University of Science and Technology Beijing, Beijing 100083, China

[c] Department of Advanced Materials Engineering, Sunmoon University, Asan-si 31460, Republic of Korea

[d] School of Advanced Materials Science and Engineering, Sungkyunkwan University, Suwon-si 16419, Republic of Korea

[e] School of Materials Science and Engineering, Beijing Institute of Technology, Beijing 100081, China

[f] Program in Semiconductor Convergence, Department of Materials Science and Engineering, Inha University, Incheon 22212, Republic of Korea

* Corresponding author. E-mail: 6120180041@bit.edu.cn (HH), dyjeong@inha.ac.kr (DYJ), jhryu@ynu.ac.kr (JR)

[1] These authors contributed equally to this work.

Phase Field Modeling

This study employed the phase field modeling of BTO-based solid solutions to explore defect-induced domain evolution, strain response, and underlying mechanisms. The spatial distribution of the spontaneous polarization vector ***P*** (with components P_1, P_2, and P_3) was used to characterize the domain structures. In contrast, the temporal dynamics of polarization were governed by the time-dependent Ginzburg–Landau (TDGL) equation. Additionally, the displacement field *u* was determined using the stress equilibrium equation.[1]

$$\begin{aligned} &\frac{\partial P_i}{\partial t} + L\frac{\delta F}{\delta P_j} = 0 \\ &\frac{\partial}{\partial x_j}\left(\sigma_{ij}(\mathbf{r},t)\right) = 0 \end{aligned} \qquad (1)$$

Here, *L* is a kinetic coefficient related to the domain wall mobility, *F* is the system's total free energy, *i.e.*, the thermodynamic driving force for polarization evolution, $\boldsymbol{\sigma_{ij}}$ is the stress tensor, and *r* and *t* are the spatial coordinate and time, respectively. The total free energy of a bulk system can be defined as follows:

$$F = F_{land}(\boldsymbol{P}) + F_{grad}(\boldsymbol{P}) + F_{elastic}(\boldsymbol{P}) + F_{elec}(\boldsymbol{P}, \boldsymbol{E}) \qquad (2)$$

Here, F includes the bulk free energy $F_{land}(\boldsymbol{P})$, domain wall energy $F_{grad}(\boldsymbol{P})$, elastic energy $F_{elastic}(\boldsymbol{P})$, and electrostatic energy $F_{elec}(\boldsymbol{P}, \boldsymbol{E})$, where *E* is the applied static electric field.

The bulk free energy density can be expanded in terms of its polarization components:

$$\begin{aligned} f_{Land} = {} & a_1(P_1^2 + P_2^2 + P_3^2) + a_{11}(P_1^4 + P_2^4 + P_3^4) + a_{12}(P_1^2P_2^2 + P_1^2P_3^2 + P_2^2P_3^2) + a_{111}(P_1^6 + P_2^6 + P_3^6) \\ & + a_{112}[P_1^4(P_2^2 + P_3^2) + P_3^4(P_2^2 + P_1^2) + P_2^4(P_3^2 + P_1^2)] + a_{123}P_1^2P_2^2P_3^2 + a_{1111}(P_1^8 + P_2^8 + P_3^8) \\ & + a_{1112}[P_1^6(P_2^2 + P_3^2) + P_3^6(P_2^2 + P_1^2) + P_2^6(P_3^2 + P_1^2)] + a_{1122}(P_1^4P_2^4 + P_1^4P_3^4 + P_2^4P_3^4) \\ & + a_{1123}(P_1^4P_2^2P_3^2 + P_1^2P_2^4P_3^2 + P_1^2P_2^2P_3^4) \end{aligned}$$

(3)

where $a_1 - a_{1123}$ are the Landau coefficients. The gradient energy density in an anisotropic system can be calculated by

$$f_{grad} = \frac{1}{2} g_{ijkl} P_{i,j} P_{k,l} \quad (4)$$

where g_{ijkl} is the gradient energy coefficient and $P_{i,j} = \frac{\partial P_i}{\partial x_j}$. The elastic energy density can be described as:

$$f_{\text{elastic}} = \frac{1}{2} c_{ijkl} e_{ij} e_{kl} = \frac{1}{2} c_{ijkl} \left(\varepsilon_{ij} - \varepsilon_{ij}^0\right)\left(\varepsilon_{kl} - \varepsilon_{kl}^0\right) \quad (5)$$

where $\mathbf{c_{ijkl}}$ is the stiffness tensor, $\mathbf{e_{ij}}$ is the elastic strain tensor, $\boldsymbol{\varepsilon_{ij}}$ is the total strain tensor, and $\boldsymbol{\varepsilon_{ij}^0}$ is the eigenstrain. The eigenstrain can be divided into two parts: the defect-induced strain $\boldsymbol{\varepsilon_{Cij}^0}$ originated from the defect dipole, and the eigenstrain from the spontaneous polarization,

$$\varepsilon_{ij}^0 = \varepsilon_{Dij}^0 + \varepsilon_{Pij}^0 = \varepsilon_{Cij}^0 + Q_{ijkl} P_{Lk} P_{Ll} \quad (6)$$

where $\boldsymbol{\varepsilon_{Pij}^0}$ is the eigenstrain for the spontaneous polarization, and $\mathbf{Q_{ijkl}}$ is the electrostrictive coefficient tensor. Here in our phase field simulation, a simple electro-strain model to account for the defect dipole was introduced:

$$\varepsilon_{Cij}^0 = Q_{\text{ijkl}}^d P_{d\text{k}} P_{d\text{l}} \quad (7)$$

where $\boldsymbol{P_d}$ is the defect polarization, and $\mathbf{Q_{ijkl}^d}$ is the corresponding electrostrictive tensor. Thus, the total strain $\boldsymbol{\varepsilon_{33}}$ can be divided into two parts, *i.e.*, one is from spontaneous polarization $\boldsymbol{P_s}$ and the other is from the defect polarization $\boldsymbol{P_d}$**:**

$$\varepsilon_{33} \approx Q_{11} P_s^2 + Q_{11}^d (P_{d0} + \Delta P_d)^2 \quad (8)$$

where $\boldsymbol{Q_{11}}$ and $\boldsymbol{Q_{11}^d}$ are the electrostriction coefficients correlated with the spontaneous polarization and defect polarization, respectively. $\boldsymbol{P_{d0}}$ is the aligned defect dipole polarization introduced by the aligned defect dipoles, and $\boldsymbol{\Delta P_d}$ is the change in defect polarization under the measurement electric field.

The electrostatic energy density f_{elec} of the system is given by,

$$f_{elec} = -P_i(r)(E_i(r) + E_{RF}(\mathrm{r})) - \frac{1}{2}P_i(r)E_i^{in}(r) \qquad (9)$$

where $\boldsymbol{E_i^{in}(r)}$ is the E-field induced by the dipole moments, $\boldsymbol{E_i(r)}$ is the applied electric field, and $\boldsymbol{E_{RF}}$ is the local electric field caused by random point defects.

The electrostatic energy density $f_{elec} = -E_iP_i - \frac{1}{2}E_i^dP_i$, where E_i is the applied electric field and E_i^d is the depolarizing electric field.

The Landau parameters of the BTO system are[2] $a_1 = 4.125\times10^5\times(\mathrm{T}-388)\ \mathrm{C}^{-2}\ \mathrm{m}^2\ \mathrm{N}$, where T is temperature in K, $a_{11} = -2.097\times10^8\ \mathrm{C}^{-4}\ \mathrm{m}^6\ \mathrm{N}$, $a_{12} = 7.974\times10^8\ \mathrm{C}^{-4}\ \mathrm{m}^6\ \mathrm{N}$, $a_{111} = 1.294\times10^9\ \mathrm{C}^{-6}\ \mathrm{m}^{10}\ \mathrm{N}$, $a_{112} = -1.95\times10^9\ \mathrm{C}^{-6}\ \mathrm{m}^{10}\ \mathrm{N}$, $a_{123} = -2.5\times10^9\ \mathrm{C}^{-6}\ \mathrm{m}^{10}\ \mathrm{N}$, $a_{1111} = 3.863\times10^{10}\ \mathrm{C}^{-8}\ \mathrm{m}^{14}\ \mathrm{N}$, $a_{1112} = 2.529\times10^{10}\ \mathrm{C}^{-8}\ \mathrm{m}^{14}\ \mathrm{N}$, $a_{1122} = 1.637\times10^{10}\ \mathrm{C}^{-8}\ \mathrm{m}^{14}\ \mathrm{N}$, $a_{1123} = 1.367\times10^{10}\ \mathrm{C}^{-8}\ \mathrm{m}^{14}\ \mathrm{N}$, $Q_{11} = 0.1\ \mathrm{C}^{-2}\ \mathrm{m}^4$, $Q_{12} = -0.034\ \mathrm{C}^{-2}\ \mathrm{m}^4$, $Q_{44} = 0.029\ \mathrm{C}^{-2}\ \mathrm{m}^4$, $c_{11} = 3.02\times10^{11}\ \mathrm{N\ m}^{-2}$, $c_{12} = 1.62\times10^{11}\ \mathrm{N\ m}^{-2}$, $c_{44} = 0.68\times10^{11}\ \mathrm{N\ m}^{-2}$, and $P_0 = |\mathbf{P}|_{T=25\ ^\circ\mathrm{C}} = 0.26\ \mathrm{C\ m}^{-2}$ is selected as the reduced unit spontaneous polarization. For defect-induced strain, a simple form of $Q_{11}^dP_{d0}\Delta P_d$ is used, where P_{d0} is assumed to be the same as the spontaneous polarization, ΔP_d was the linearity correlated with the P_{d0}, $Q_{11}^d = 0.15$. The simulation scale is 256 dx $\times$ 256 dz, and the grid scales dx and dz are 1 nm. The Fourier method was used for solving the equations.

Table S1. Comparison of materials, property changes, and aging conditions related to thermal aging effects in ferroelectric materials.[3-14]

Materials	Unaged		Aged		Aging Condition	Reference
	P-E	***S-E***	***P-E***	***S-E***		
0.3 mol% Mn-doped $BaTiO_3$ single crystal	Single [a]	0.2% (10 kV cm^{-1})	Double [b]	0.4% (10 kV cm^{-1})	80 °C, 2 weeks	[3]
Aged 0.5 mol% Mn-doped $BaTiO_3$ single crystal	Single	0.03% (7 kV cm^{-1})	Double	0.12% (13 kV cm^{-1})	25 °C, 134 days	[4]
Fe-doped $BaTiO_3$ single crystal	Single	-	Double	0.75% (2 kV cm^{-1})	80 °C, 5 days	[5]
0.2 mol% Fe-doped $0.62Pb(Mg_{1/3}Nb_{2/3})O_3$-0.38PbTiO3 single crystal	Single	0.05% (12.5 kV cm^{-1})	Double	0.8% (12.5 kV cm^{-1})	140 °C, 1 week	[6]
1.0 mol% Mn-doped $(Ba_{0.95}Sr_{0.05})TiO_3$ ceramic	Single	0.06% (30 kV cm^{-1})	Double	0.12% (30 kV cm^{-1})	25 °C, 4 weeks	[7]
$K[(Nb_{0.9}Ta_{0.1})_{0.99}Mn_{0.01}]O_3$ ceramic	Single	0.06% (50 kV cm^{-1})	Double	0.16% (50 kV cm^{-1})	130 °C, 5 days	[8]
$0.6(BaTi_{0.8}Ca_{0.2}O_3)$-$0.4(Ba_{0.7}Ca_{0.3}TiO_3)$ ceramic	Single	0.125% (30 kV cm^{-1})	Double	0.175% (30 kV cm^{-1})	22 °C, 4 weeks	[9]
1.0 mol% Cu-doped $(K_{0.5}Na_{0.5})NbO_3$ ceramic	Single	0.15% (60 kV cm^{-1})	Double	0.25% (60 kV cm^{-1} kV cm^{-1})	25 °C, 1 year	[10]
1.5 mol% Fe-doped $(Pb_{0.95}Ba_{0.025}Sr_{0.025})(Zr_{0.53}Ti_{0.47})O_3$ ceramic	Single	0.075% (30 kV cm^{-1})	Double	0.325% (30 kV cm^{-1})	25 °C, 3 months	[11]
$(Bi_{0.5}Na_{0.5})_{0.852}(Bo_{0.5}K_{0.5})_{0.11}Ba_{0.038}Ti_{0.9875}Nb_{0.0125}O_3$ ceramic	Single	0.38% (60 kV cm^{-1})	Double	0.41% (60 kV cm^{-1})	80 °C, 2 weeks	[12]
$K_{0.5}Na_{0.5}NbO_3$-$K_{5.4}Ci_{1.3}Ta_{10}O_9$ ceramic	Single	-	Double	-	80 °C, 70 days	[13]
$Ba(Ti_{0.99}Mn_{0.01})O_3$ ceramic	Single	-	Double	-	80 °C, 37 days	[14]

[a] Single: Single hysteresis loop

[b] Double: Double hysteresis loop

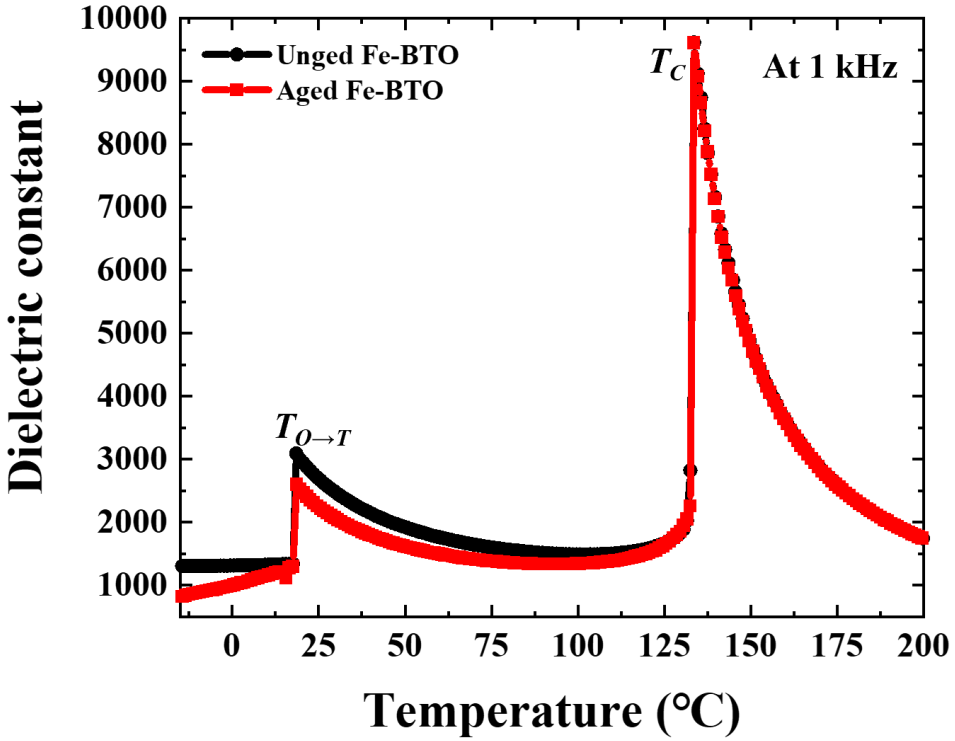

Figure S1. Dependence of the dielectric constant on temperature in Fe-doped $BaTiO_3$ single crystal (Fe-BTO). Temperature dependence of dielectric constant in unaged (red line) and aged (black line) Fe-BTO. Significant variations in dielectric constant at 20 °C is for the temperature for phase transition from orthorhombic to tetragonal; $T_{O\rightarrow T}$ and 130 °C is for the temperature for phase transition from tetragonal to cubic phase; T_C.

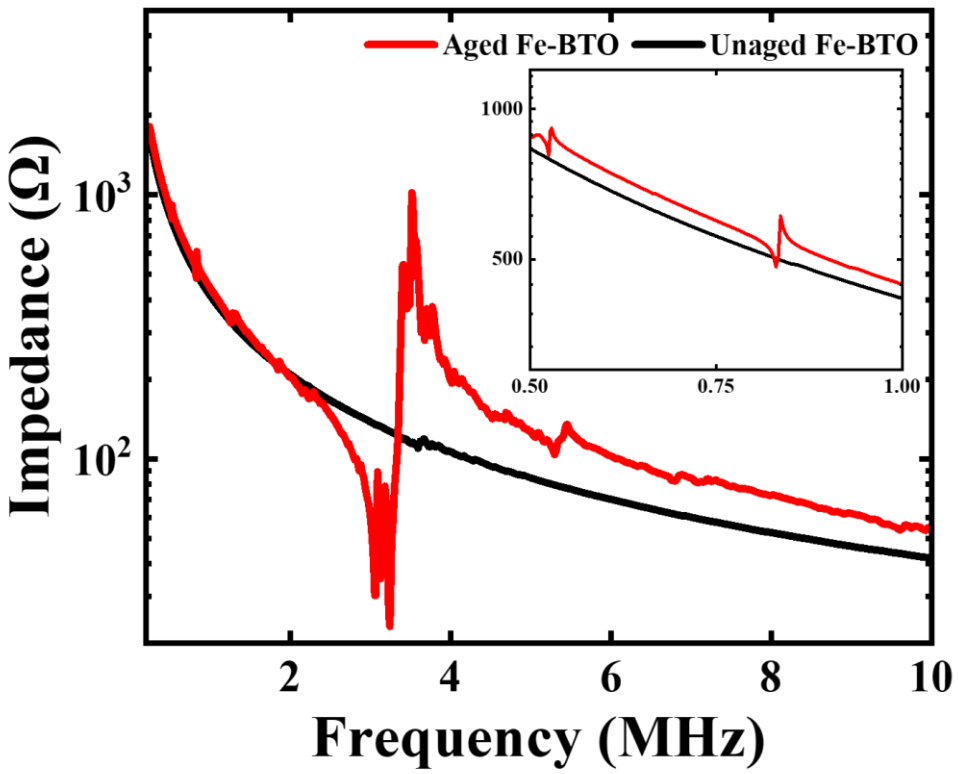

Figure S2. Impedance spectra of the aged (red) and unaged (black) Fe-BTO. Impedance spectra of aged Fe-BTO and unaged Fe-BTO confirmed that a resonance spectrum appears in the 0.5–1 MHz band at inset graph and in the 3–4 MHz band after aging. Based on these resonance spectrum peaks, self-poling is assumed to have occurred due to the defect dipoles.

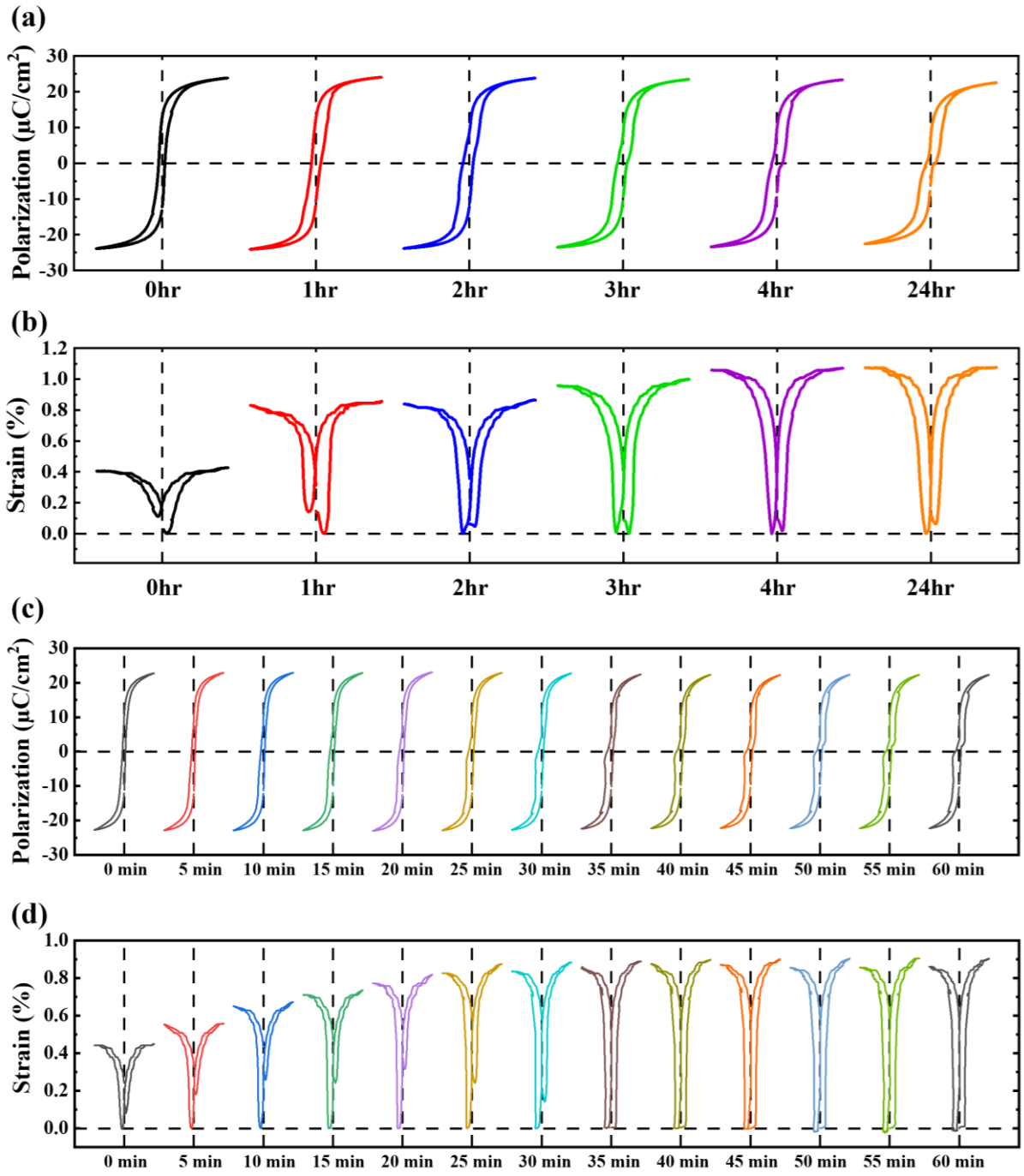

Figure S3. Evolution of *P-E* and *S-E* hysteresis over time after an AC electric field is applied for activation. The results of *P-E* and *S-E* when an electric field (10 Hz, 3 kV mm^{-1}) is applied (a)–(b) at 1 hour intervals and (c)–(d) at 5 minute intervals. According to the results, the more times the AC electric field is applied within the same time, the faster the aging phenomenon becomes.

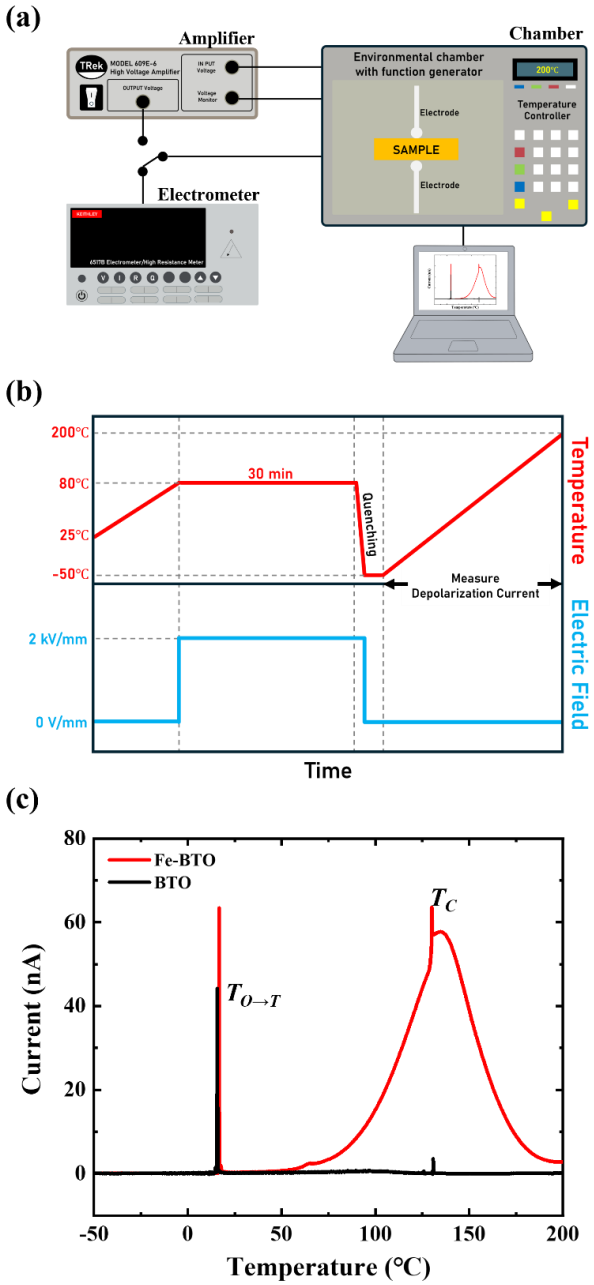

Figure S4. Schematic and results for thermally stimulated depolarization current (TSD C) measurement. (a) Schematic of TSDC measurement setup and (b) temperature and electrical process curves showing polarization and depolarization during the TSDC me asurement. (c) TSDC results for the Fe-BTO and BTO. The sharp peaks observed at 20° C and 130°C are confirmed to be due to changes in the crystal structure, as compare d with Figure SI in the SI. The broad variation in Fe-BTO from approximately 50°C to 200°C is presumed to result from current peaks caused by the de-poling of oxygen

vacancies that were displaced during poling and were subsequently depolarized as the temperature increased. The calculated oxygen vacancy concentrations in Fe-BTO and BTO are approximately $6.27 \times 10^{14}\,cm^{-3}$ and $1.1 \times 10^{13}\,cm^{-3}$, respectively.[15]

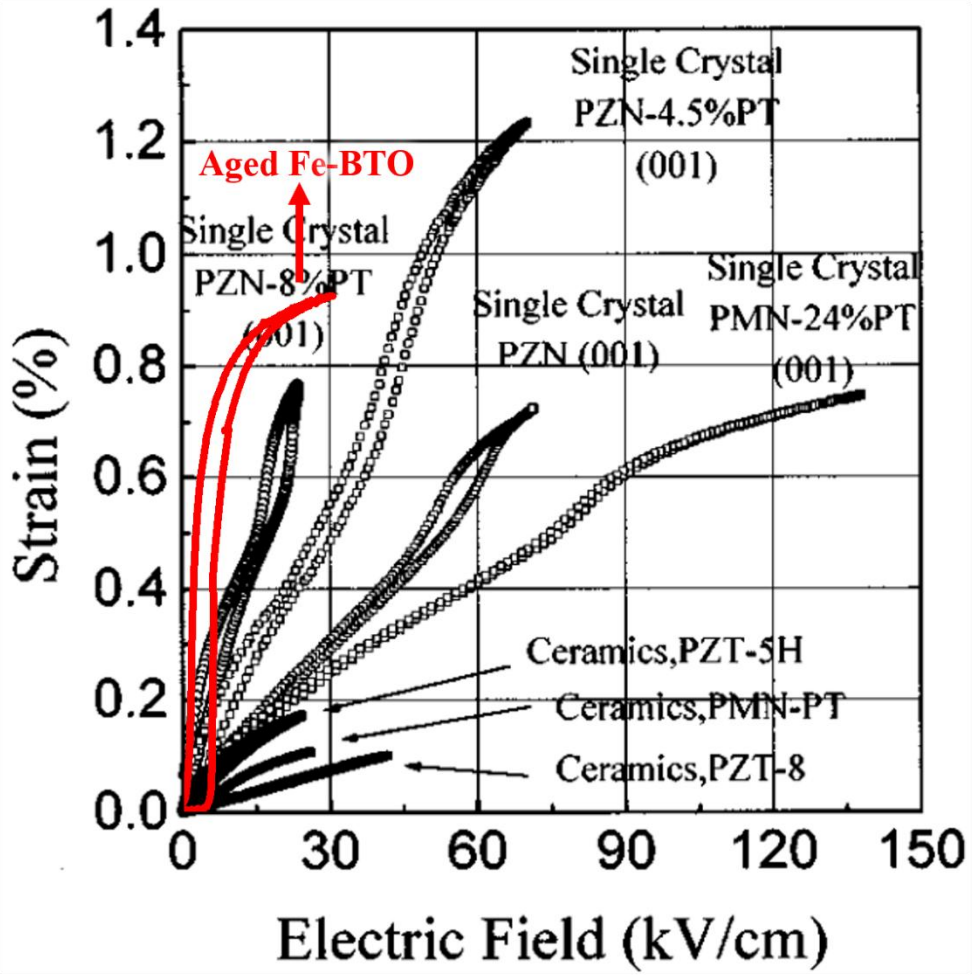

Figure S5. Comparison of electro-strain characteristics between reported lead piezoelectric single crystals and aged Fe-BTO. The red line in the graph represents the gigantic deformation of Fe-BTO after aging.[16]

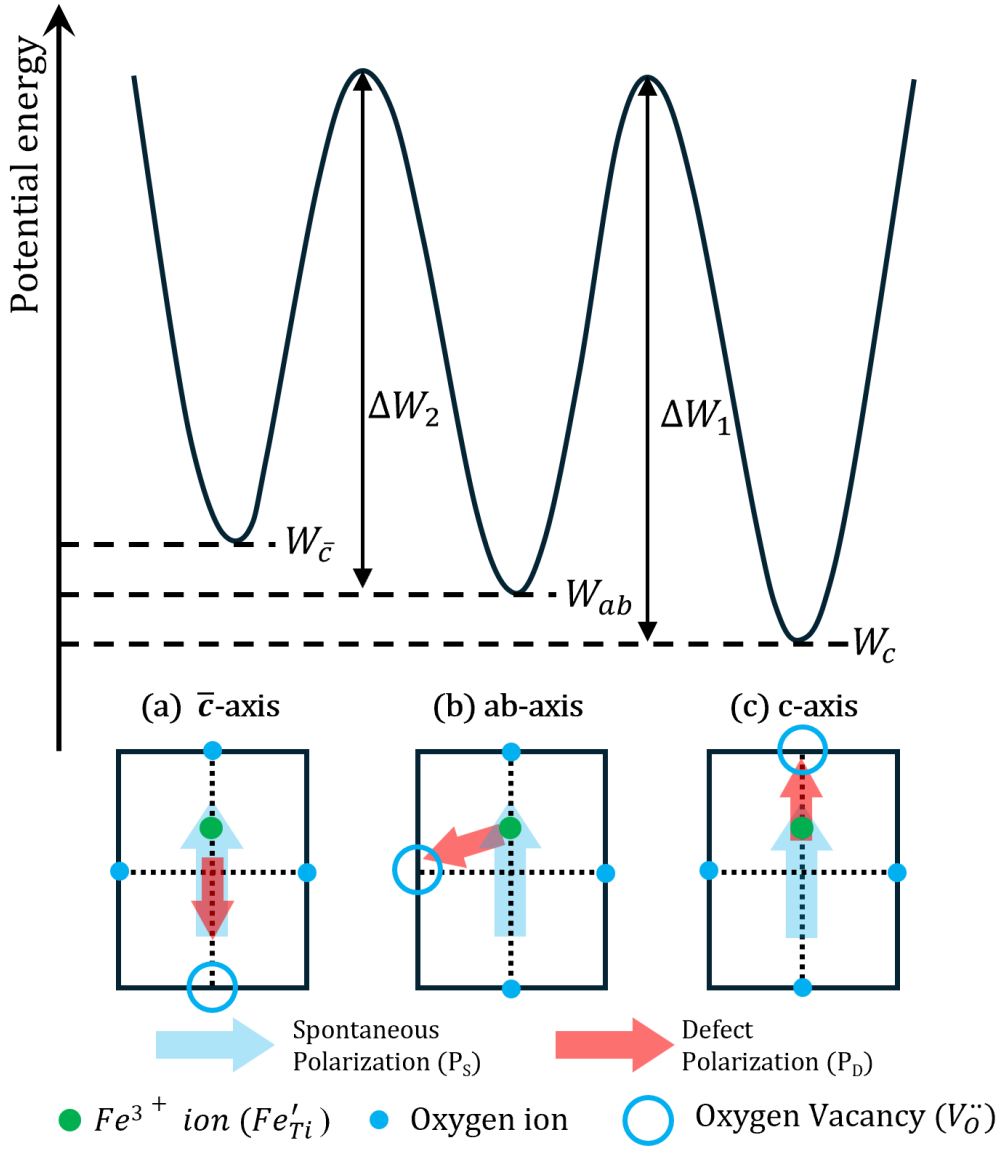

Figure S6. Schematic of potential energy of defect polarization according to the location of oxygen vacancies in tetragonal perovskite-structured ferroelectric unit cell.[17,18]

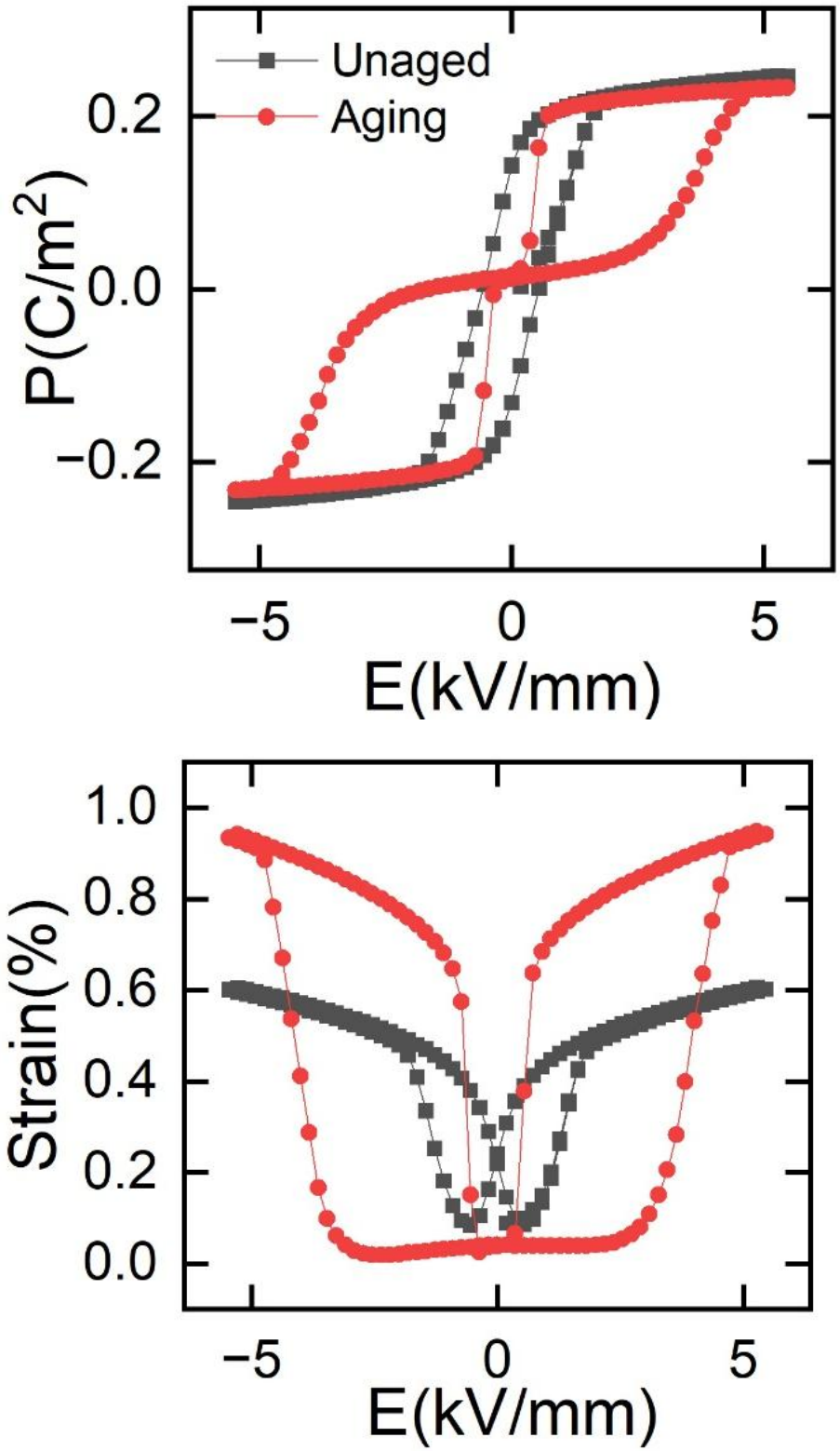

Figure S7. Phase field simulation of *P-E* loop and *S-E* loop with unaged and aged F e-BTO single crystals.

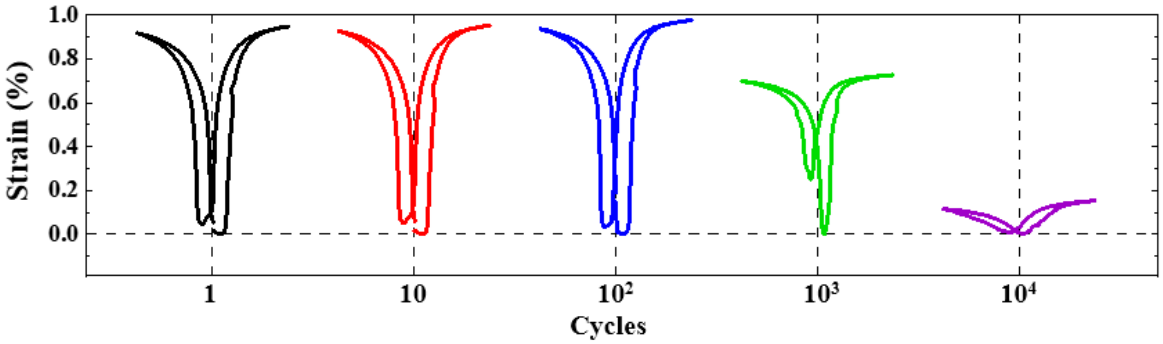

Figure S8. Evolution of S-E hysteresis loops for aged Fe-BTO during 10^4 AC electric field cycles (10 Hz, 3 kV mm^{-1})

References

[1] Y. L. Li, S. Y. Hu and L. Q. Chen, J. Appl. Phys., 2005, 97, DOI: 10.1063/1.1849820

[2] Y. L. Li, L. E. Cross and L. Q. Chen, J. Appl. Phys., 2005, 98, DOI: 10.1063/1.2042528

[3] L. Zhang and X. Ren, Phys. Rev. B, 2006, 73, DOI: 10.1103/PhysRevB.73.094121

[4] R. A. Maier, T. A. Pomorski, P. M. Lenahan and C. A. Randall, J. Appl. Phys., 2018, 118, DOI: 10.1063/1.4934505

[5] Ren X, Nat. Mater., 2004, 3, 91-94

[6] Z. Feng, O. K. Tan, W. Zhu, Y. Jia and H. Luo, Appl. Phys. Lett., 2008, 92, DOI: 10.1063/1.2908230

[7] L. X. Zhang, W. Chen and X. Ren, Appl. Phys. Lett., 2004, 85, 5658-5660

[8] Z. Feng and S. W. Or, J. Alloys Compd., 2009, 480, L29-L32

[9] Y. Yang, Z. Zhou, L. Xin, C. Zhou, L. Zhang, A. Xiao and X. Ren, J. Phys. Chem. C , 2019, 123, 3321-3325

[10] J. Hao, Z. Xu, R. Chu, W. Li, J. Du, P. Fu and G. Li, J. Am. Ceram. Soc., 2016, 99, 402-405

[11] X. Zhao, R. Liang, W. Zhang, G. Wang and X. Dong, Appl. Phys. Lett., 2014, 105, DOI: 10.1063/1.4905359

[12] J. Feng, R. Huang, Z. Liang, Z. Du, Y. Dai, J. Wu and H. Lin, Ceram. Int., 2022, 48, 2355-2361

[13] D. Lin, K. W. Kwok and H. W. L. Chan, J. Am. Ceram. Soc., 2009, 92, 1362-1365

[14] Y. Y. Guo, Y. Zhao, H. G. Zhang and N. Zhang, J. Alloys Compd., 2017, 696, 814–819

[15] H. Song, J. Goud, J. Ye, W. Jung, J. Ji and J. Ryu, J. Korean Ceram. Soc., 2023, 60, 747-759

[16] S. E. Park and T. R. Shrout, J. Appl. Phys., 1997, 82, 1804-1811

[17] P. Erhart, R. A. Eichel, P. Träskelin and K. Albe, Phys. Rev. B, 2007, 76, DOI: 10.1103/PhysRevB.76.174116

[18] R. A. Eichel, Phys. Chem. Chem. Phys., 2011, 13, 368-384